Mater. Res. Soc. Symp. Proc. Vol. 1164 © 2009 Materials Research Society 1164-L09-10

Origins of Twinned Microstructures in $B_{12}As_2$ Epilayers Grown on (0001) 6H-SiC and Their Influence on Physical Properties

Yu Zhang[1], Hui Chen[1], Ning Zhang[1], Michael Dudley[1], Yinyan Gong[2], Martin Kuball[2], Zhou Xu[3], Yi Zhang[3], James H. Edgar[3], Lihua Zhang[4], Yimei Zhu[4]

[1]Department of Materials Science and Engineering, Stony Brook University, Stony Brook, NY 11794-2275

[2]H.H. Wills Physics Laboratory, University of Bristol, Bristol, United Kingdom

[3]Department of Chemical Engineering, Kansas State University, Manhattan, KS

[4]Center for Functional Materials, Brookhaven National Laboratory, Upton, NY

ABSTRACT

The defect structure in $B_{12}As_2$ epitaxial layers grown at two different temperatures on (0001) 6H-SiC by chemical vapor deposition (CVD) was studied using synchrotron white beam x-ray topography (SWBXT) and high resolution transmission electron microscopy (HRTEM). The observed differences in microstructures were correlated with the differences in nucleation at the two growth temperatures. The effect of the difference in microstructure on macroscopic properties of the $B_{12}As_2$ was illustrated using the example of thermal conductivity which was measured using the 3-ω technique. The relationship between the measured thermal conductivity and observed microstructures is discussed.

INTRODUCTION

$B_{12}As_2$ is a member of the icosahedral boride family with a structure consisting of twelve boron atom icosahedra arranged at the corners of a rhombohedral unit cell with two-atom As-As chains along the body diagonal. It has a band gap of 3.47eV, and the material has the extraordinary ability to "self-heal" after radiation damage, making it potentially useful for devices operating in high electron radiation environments [1-6]. The absence of native substrates necessitates the heteroepitaxial growth of $B_{12}As_2$, typically on 6H-SiC substrates, often achieved using chemical vapor deposition [7]. Epitaxial growth on (0001) 6H-SiC is facilitated by the fact that the in-plane lattice constants of 6H-SiC are close to one half of those of $B_{12}As_2$. Gaining a detailed understanding of its microstructure is essential on the pathway to device demonstration. In this paper, we present studies of the influence of growth temperature on the microstructure of $B_{12}As_2$ thin films grown on (0001) 6H-SiC substrates. Implications of the microstructure on selected macroscopic physical properties are discussed.

EXPERIMENT

On axis, c-plane 6H-SiC wafers were used as substrates for the CVD growth of $B_{12}As_2$. The $B_{12}As_2$ films were synthesized by employing gaseous precursors of 1% B_2H_6 in H_2 and 2% AsH_3 in H_2. The c-plane $B_{12}As_2$ was deposited at 1275°C and 1450°C, for samples, denoted here S1 and S2, respectively, with 500 Torr of reactor pressure. Non-destructive SWBXT was carried out

at the Stony Brook Topography station at the National Synchrotron Light Source, Brookhaven National Laboratory. Following this, cross-sectional TEM samples were made parallel to $(\mathbf{11\bar{2}0})_{6H\text{-}SiC}$. Conventional and high resolution TEM observation was performed using a JEOL 2100 transmission electron microscope with an electron accelerating voltage of 200KeV. To illustrate the implication of the microstructure on macroscopic physical properties of the film, the example of thermal conductivity was considered, measured using the 3-ω technique， which is extensively used to measure thermal conductivities of bulk and thin film dielectric materials [8-9]. An ~100nm thick silicon oxide film was deposited onto the $B_{12}As_2$ film by plasma enhanced CVD to electrically isolate the sample. After this, photolithography was used to define a pattern of metal line heaters followed by the sputter deposition of the metal. An AC voltage of frequency ω was applied to the line heater, resulting in an increase in temperature. Because the resistivity of the metal depends on temperature, the voltage along the line heater also changes. The 3ω component in the resulting AC voltage was measured, which can be used to calculate the thermal conductivity.

RESULTS AND DISCUSSION

Figure 1 shows the indexed diffraction patterns of sample S1 and S2 obtained via SWBXT in transmission using a $1mm^2$ area incident white beam. The diffraction spots labeled using the four index system correspond to the 6H-SiC substrate and exhibit six-fold symmetry as expected. For both samples, exposure times were increased in order to allow the weaker $B_{12}As_2$ diffraction spots to accumulate sufficient exposure to enable indexing. The diffraction spots from the $B_{12}As_2$ were generally more diffuse and appeared to form a 6-fold symmetric pattern rather than the 3-fold symmetric pattern expected for the rhombohedral crystal structure of $B_{12}As_2$. Detailed analysis confirms that this is because both films were twinned and, using the three index system, subscripts I and II are used to indicate matrix and twin diffraction spots. The size and shape of the matrix and twin diffraction spots indicate that the films appear to be fairly homogeneous solid solutions of matrix and twin.

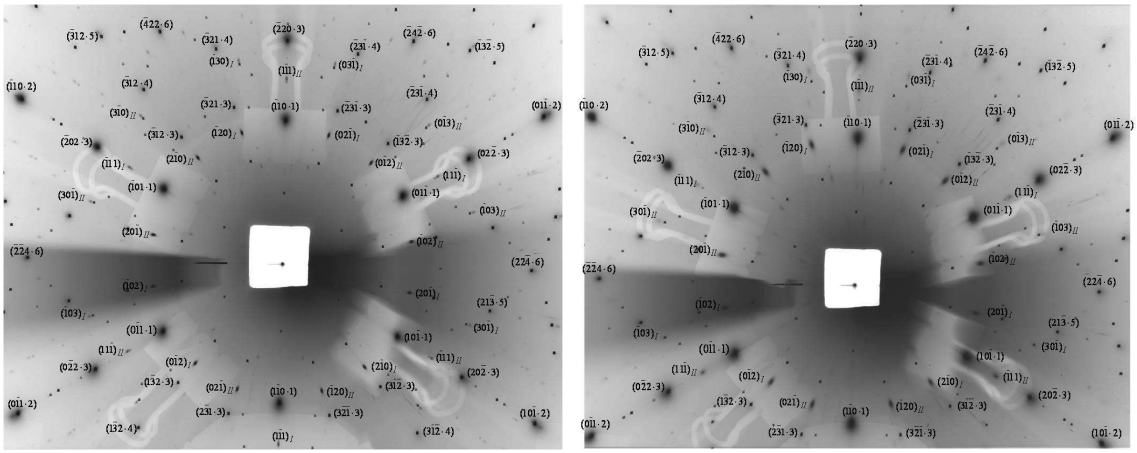

Figure 1. Indexed diffraction patterns of S1 and S2.

The presence of rotational variants in the form of twins is expected in such degenerate epitaxy, as a lower symmetry film is epitaxially grown on a higher symmetry substrate, and the rotational variants are related by the symmetry element present in the substrate which is absent in the film. [10-13]. The details of the microstructure of the twin domains are, however, expected to

vary with growth temperature. In order to explore this variation in more detail, both samples were studied using TEM and conventional TEM images recorded from the samples are shown in Figures 2-4. In sample S1, sets of long, parallel (111) twin boundaries are confined to a region ~200nm thick comprising the volume from the substrate/epilayer interface to about one half of the thickness of the epilayer. The average thickness of the twin domains separated by the neighboring twin boundaries is around 60nm (see schematic diagram of the microstructure in Figure 2(c)). In sample S2, twin boundaries (lateral in this case) are mostly perpendicular to the epilayer interface, and the average distance between neighboring lateral twin boundaries (width of one domain) is around 140nm. (See schematic diagram of the microstructure in Figure 2(d))

Enlarged HRTEM images recorded from samples S1 and S2 are shown in Figures 3 and 4, respectively. Figure 3 shows a (111) twin boundary separating two twinned domains. This and other such boundaries have slightly increased complexity in their images since not only are they stepped parallel to the interface on these images but also into the plane of the page. Figure 4 shows a fairly complex microstructure comprising an almost columnar domain configuration suggesting that it may originate due to multiple nucleation. Note that the interface in both samples exhibits steps of opposite sign as expected for these "on-axis" substrates.

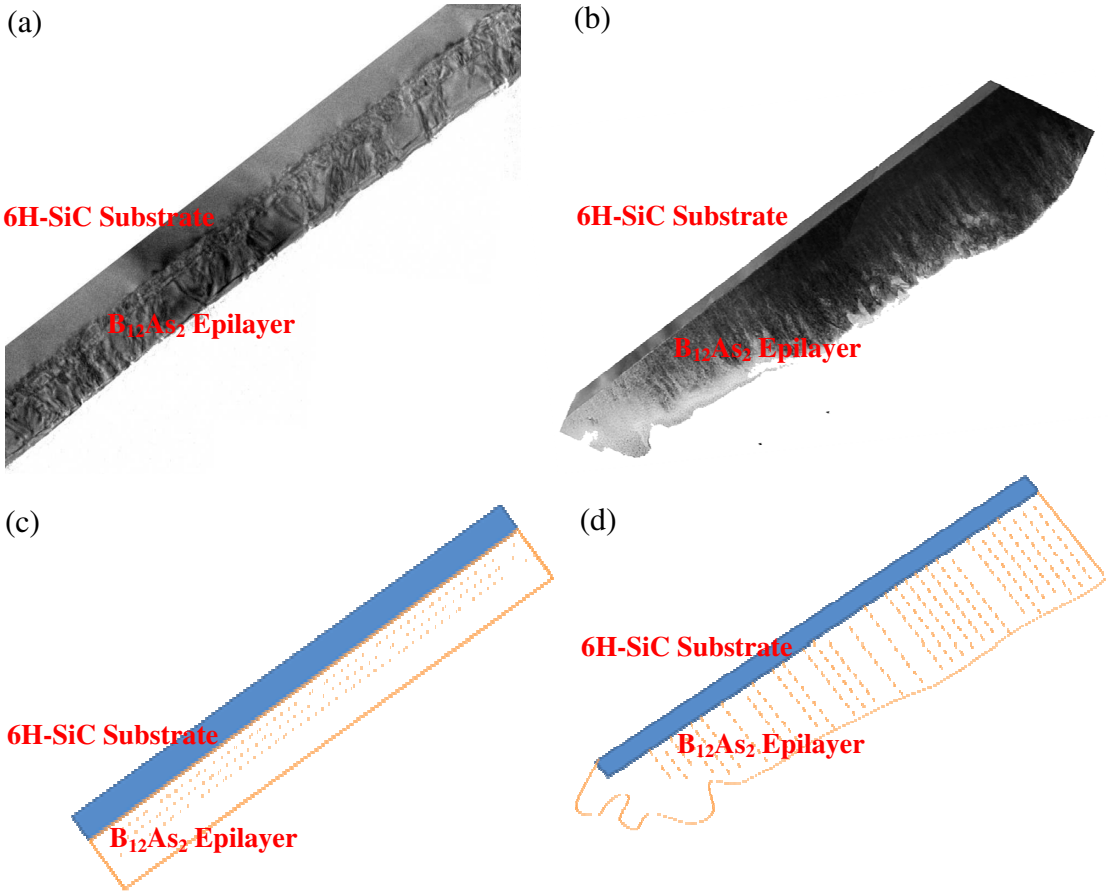

Figure 2. Low magnification TEM images of epilayers in S1 ((a)) and S2 ((b)). Note the boundaries between twinned domains approximately parallel to the interface in the interface region in (a) and penetrating the epilayer perpendicular to the interface in (b). Schematic diagram of epilyaers in S1((c)) and S2 ((d)). Dotted lines indicate twin boundaries.

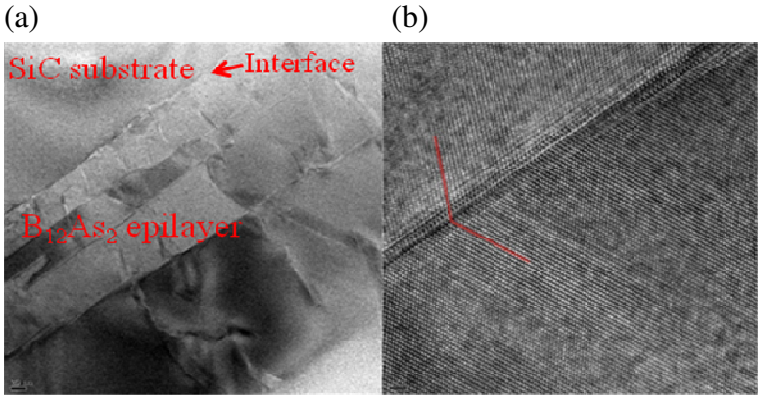

Figure 3. Enlarged TEM image of the twin boundaries parallel to the interface in sample S1 ((a) and HRTEM image of one of the (111) boundaries ((b)).

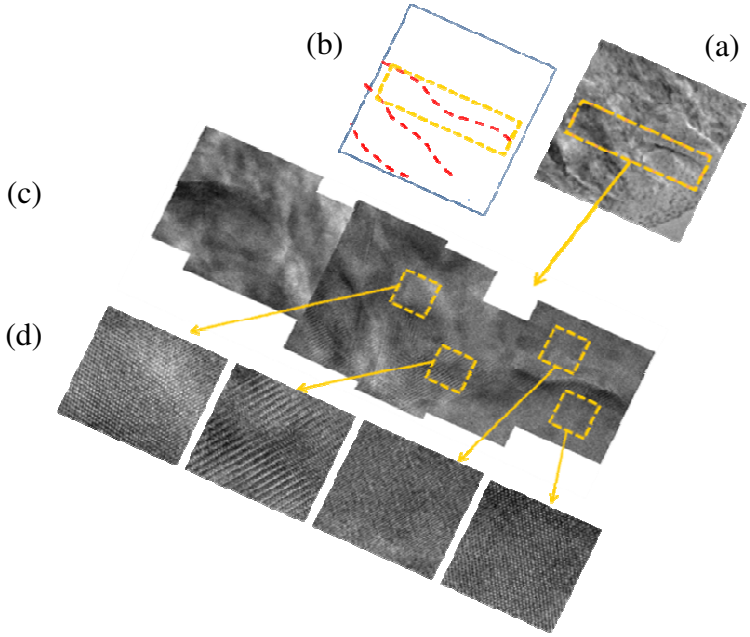

Figure 4. Enlarged TEM image of the lateral twin boundaries in sample S2 ((a) and (c)) and schematic diagram ((b)). HRTEM images of the indicated regions both matrix and twin domains ((d)).

Some understanding of the origin of these quite different microstructures can be obtained by consideration of the different nucleation under the two sets of growth conditions. Most growth parameters are similar except for the growth temperature which is 1275 °C for S1 and 1450 °C for S2. One might intuitively expect that the lower growth temperature would create a higher super saturation and thus a higher nucleation rate. However, contrary to expectation, the sample which appears to exhibit a microstructure resulting from multiple nucleation effects is sample S2 which was grown at the higher temperature. Insight into this can be provided by consideration of the species likely involved in the CVD growth. For the 1% B_2H_6 and 2% AsH_3 in H_2 precursors utilized one might expect gas phase reaction at the growth temperature to involve species such as icosahedral $B_{12}H_{12}$ reacting with arsine to form small subsets of the $B_{12}As_2$ unit cell [13]. Given the relatively large size of these resultant species, it seems reasonable to assume that their surface diffusion will be complex and that they might be subject to the "lock-and-key" effect valid for

the surface diffusion of large organic molecules on metal substrates [14]. For such systems only those molecules adsorbed onto the surface that are not oriented correctly to form bonds to the surface have the opportunity to become mobile and diffuse. If they are oriented and positioned to form bonds (multiple bonds) they are locked onto the surface and become immobile. Thus, in such systems, surface diffusion is a greater barrier to the nucleation process than thermodynamics. For the growth of $B_{12}As_2$ epilayers grown on on-axis (0001) 6H-SiC substrates, species can bond to the substrate in either "matrix" or "twin" orientation [12] and species are most effectively "locked-in" if they are able to bond simultaneously to a terrace and a step riser [12-13].

For sample #S1, the lower growth temperature of 1275°C leads to higher super-saturation but also more difficult surface diffusion compounded by the large size of the species. Thus, it is expected that more species will drop onto the surface but once there they will not undergo much surface diffusion. Only those that happen to drop in the right orientation close to a step riser will be locked in by bonding to both terrace and riser with all other being expected to desorb. Those that lock in will develop into nuclei and expand sideways until they impinge upon adjacent nuclei which may be in matrix or twin orientation. Since, the probability of such fortuitous adsorption is relatively low, this will lead to just a few nuclei being formed which will then coalesce and over grow each other to form a relatively small number of domains separated by twin boundaries roughly parallel to the interface consistent with the microstructure observed in sample S1.

For sample #S2, the higher growth temperature of 1450°C leads to lower super-saturation but easier surface diffusion which means that while fewer species will drop onto the surface but those that do are able to experience more surface diffusion. Some species, as at the lower temperature, may by chance be correctly positioned and oriented to immediately bond to terrace and riser while the majority will have the chance to diffuse around until they find a step, get locked in and form a nucleus (still others who don't find a step will desorb). Therefore, in this case, in contrast to the lower temperature case, it is more likely that we will have multiple nucleation and smaller domains leading to a larger number of nuclei which impinge upon each other at an earlier stage of growth which will be separated by many complex twin domain walls roughly perpendicular to the interface. This is consistent with the microstructure observed in sample S2.

To illustrate the implication microstructures have on macroscopic physical properties of the $B_{12}As_2$, preliminary measurements of the thermal conductivity of the $B_{12}As_2$ along the $[111]_{B12As2}$ direction, i.e., perpendicular to the film surface, were performed using the 3-ω technique. To measure thermal conductivity of thin film, one-dimension heat conduction model and semi-infinite substrate are assumed. Qualitatively, it has been estimated that the errors related to these two factors are within 1% when the thermal penetration depth is at least 5 times greater than the width of the line heater and smaller than one-fifth of the sample thickness. Both conditions are fully satisfied in the frequency range used in our experiments [15]. We determined at room temperature a thermal conductivity of 0.148 $Wcm^{-1}K^{-1}$ for sample S1 and 0.256 $Wcm^{-1}K^{-1}$ for sample S2. This difference is in part due to the difference in microstructure for both samples, with S1 having a larger density of grain boundaries/domain walls than S2 parallel to the sample surface. Thermal conductivity is affected by phonon scattering occurring at these twin or grain boundaries and will diminish thermal conductivity more for sample S1 than S2. One of the potential application of IBA is for thermoelectrics. The conversion efficiency from heat to electricity depends on the figure-of-merit, which is inverse proportional to thermal

conductivity, and proportional to product of the square of thermal power and electrical conductivity. For this purpose, we want material with low thermal conductivity. The HRTEM results help to understand how to manipulate the thermal conductivity by varying growth condition. People have been working on develop complex material with low thermal conductivity and high thermal power. Further contributions to difference in thermal conductivity may arise from differences in the impurity concentration. A detailed analysis will be reported elsewhere [16].

CONCLUSIONS

The defect structures in $B_{12}As_2$ epitaxial layers grown at two different temperatures on (0001) 6H-SiC by chemical vapor deposition (CVD) was studied using synchrotron white beam x-ray topography (SWBXT) and high resolution transmission electron microscopy (HRTEM). Differences in the observed microstructures were correlated with difference in nucleation at different growth temperature arising from the "lock-and-key" effect. We show that macroscopic physical properties of the $B_{12}As_2$ are affected by the microstructure, as illustrated by the example of thermal conductivity.

ACKNOWLEDGEMENT

The authors gratefully acknowledge support by the National Science Foundation (Materials World Network) under Grant No.0602875 and by the Engineering and Physical Science Research Council (EPSRC) under Grant No. EP/D075033/1 under the NSF-EPSRC Joint Materials Program. The X-ray topography experiments have been carried out at Stony Brook Topography Facility (Beamline X19C) at the National Synchrotron Light Source (NSLS), Brookhaven National Laboratory (BNL), which is supported by the U.S. Department of Energy (D.O.E.) under Grant No. DE-AC02-76CH00016. Research carried out in part at the Center for Functional Nanomaterials, BNL, which is supported by the U.S. D.O.E., Division of Materials Sciences and Division of Chemical Sciences, under contract No. DE-AC02-98CH10886. We thank J. Gray (University of Bristol) for contributions to this work.

REFERENCES

1. D. Emin, *Physics Today*, **55**, January (1987).
2. D. Emin, *J. Sol. Sta. Chem.*, **179**, 2791 (2006).
3. D. Emin, T. L. Aselage, *J. App. Phys.*, **97**, 013529 (2005).
4. D. Emin, *J. Sol. Sta. Chem.*, **177**, 1619 (2004).
5. M. Carrard, D. Emin, L. Zuppiroli, *Phys. Rev. B*, **51**(17), 11270 (1995).
6. T.L. Aselage and D. Emin, Boron Carbides, in CRC Handbook of Thermoelectrics, D.M. Rowe (Ed.), CRC Press, Boca Raton, (1995).
7. R. Nagarajan, Z. Xu, J. H. Edgar, F. Baig, J. Chaudhuri, Z. Rek, E. A. Payzant, H. M. Meyer, J. Pomeroy and M. Kuball, *J. Crystal Growth.*, **273**, 431 (2005).
8. Cahill and Pohl, *Phys. Rev.*, B **35**, 4067 (1987)
9. Cahill et al., *Rhys. Rev.*, B **50**, 6077 (1994)
10. S. W. Chan, *J. Phys. Chem. Solids*, **55**, 1137 (1994).
11. C. P. Flynn and J. A. Eades, *Thin Solid Films*, **389**, 116 (2001).
12. H. Chen, G. Wang, M. Dudley, L. Zhang, L. Wu, Y. Zhu, Z. Xu, J. H. Edgar, and M. Kuball**,** *J. Appl. Phys.*, 103 (12), 123508 (2008)
13. Hui Chen, Guan Wang, Michael Dudley, Zhou Xu, J. H. Edgar, Tim Batten, Martin Kuball,

Lihua Zhang, and Yimei Zhu, *Appl. Phys. Lett.*, 92 (23), 231917 (2008)
14. Roberto Otero, Frauke Hümmelink, Fernando Sato, Sergio B. Legoas, Peter Thostrup, Erik Lægsgaard, Ivan Stensgaard, Douglas S. Galvão and Flemming Besenbacher, *Nature Materials*, **3**, 779 - 782 (2004)
15. T. Borca-Tasciuc et al., *Review of Scientific Instruments*, 72, 2139 (2001)
16. Y. Gong, J. Gary, H. Chen, Yu Zhang, M. Dudley, Yi Zhang, J. Edgar, and M. Kuball, (unpublished).